Probabilistic functional tractography of the human cortex revisited

Trebaul, Lena

2018-11-01

Trebaul , L , Deman , P , Tuyisenge , V , Jedynak , M , Hugues , E , Rudrauf , D , Bhattacharjee , M , Tadel , F , Chanteloup-Foret , B , Saubat , C , Mejia , G C R , Adam , C , Nica , A , Pail , M , Dubeau , F , Rheims , S , Trebuchon , A , Wang , H , Liu , S , Blauwblomme , T , Garces , M , De Palma , L , Valentin , A , Metsähonkala , E-L , Petrescu , A M , Landre , E , Szurhaj , W , Hirsch , E , Valton , L , Rocamora , R , Schulze-Bonhage , A , Mindruta , I , Francione , S , Maillard , L , Taussig , D , Kahane , P & David , O 2018 , ' Probabilistic functional tractography of the human cortex revisited ' , NeuroImage , vol. 181 , pp. 414-429 . https://doi.org/10.1016/j.neuroimage.2018.07.039

http://hdl.handle.net/10138/247815
https://doi.org/10.1016/j.neuroimage.2018.07.039

NeuroImage 181 (2018) 414–429

Contents lists available at ScienceDirect

NeuroImage

journal homepage: www.elsevier.com/locate/neuroimage

Probabilistic functional tractography of the human cortex revisited

Lena Trebaul [a,b], Pierre Deman [a,b], Viateur Tuyisenge [a,b], Maciej Jedynak [a,b], Etienne Hugues [a,b], David Rudrauf [a,b], Manik Bhattacharjee [a,b], François Tadel [a,b], Blandine Chanteloup-Foret [a,b], Carole Saubat [a,b], Gina Catalina Reyes Mejia [a,b], Claude Adam [c], Anca Nica [d], Martin Pail [e], François Dubeau [f], Sylvain Rheims [g], Agnès Trébuchon [h], Haixiang Wang [i], Sinclair Liu [j], Thomas Blauwblomme [k], Mercedes Garcés [l], Luca De Palma [m], Antonio Valentin [n], Eeva-Liisa Metsähonkala [o], Ana Maria Petrescu [p], Elizabeth Landré [q], William Szurhaj [r], Edouard Hirsch [s], Luc Valton [t], Rodrigo Rocamora [u], Andreas Schulze-Bonhage [v], Ioana Mindruta [w], Stefano Francione [x], Louis Maillard [y], Delphine Taussig [z], Philippe Kahane [a,b,aa], Olivier David [a,b,*]

[a] Inserm, U1216, Grenoble, F-38000, France
[b] Univ. Grenoble Alpes, Grenoble Institut des Neurosciences, GIN, Grenoble, F-38000, France
[c] Epilepsy Unit, Dept of Neurology, Pitié-Salpêtrière Hospital, APHP, Paris, France
[d] Neurology Department, CHU, Rennes, France
[e] Brno Epilepsy Center, Department of Neurology, St. Anne's University Hospital and Medical Faculty of Masaryk University, Brno, Czech Republic
[f] Montreal Neurological Institute and Hospital, Montreal, Canada
[g] Department of Functional Neurology and Epileptology, Hospices Civils de Lyon and University of Lyon, Lyon, France
[h] Service de Neurophysiologie Clinique, APHM, Hôpitaux de la Timone, Marseille, France
[i] Yuquan Hospital Epilepsy Center, Tsinghua University, Beijing, China
[j] Canton Sanjiu Brain Hospital Epilepsy Center, Jinan University, Guangzhou, China
[k] Department of Pediatric Neurosurgery, Hôpital Necker-Enfants Malades, Université Paris V Descartes, Sorbonne Paris Cité, Paris, France
[l] Multidisciplinary Epilepsy Unit, Hospital Universitario y Politécnico La Fe, Valencia, Spain
[m] Department of Neuroscience, Bambino Gesù Children's Hospital, IRRCS, Rome, Italy
[n] Department of Basic and Clinical Neuroscience, Institute of Psychiatry, Psychology & Neuroscience (IoPPN), London, UK
[o] Epilepsy Unit, Hospital for Children and Adolescents, Helsinki, Finland
[p] Neurophysiology and Epilepsy Unit, Bicêtre Hospital, France
[q] Department of Neurosurgery, Sainte-Anne Hospital, Paris, France
[r] Epilepsy Unit, Department of Clinical Neurophysiology, Lille University Medical Center, Lille, France
[s] University Hospital, Department of Neurology, Strasbourg, France
[t] University Hospital, Department of Neurology, Toulouse, France
[u] Epilepsy Monitoring Unit, Department of Neurology, Hospital del Mar-IMIM, Barcelona, Spain
[v] Epilepsy Center, Medical Center – University of Freiburg, Faculty of Medicine, University of Freiburg, Germany
[w] Neurology Department, University Emergency Hospital, Bucharest, Romania
[x] Epilepsy Surgery Center Niguarda Hospital, Milan, Italy
[y] Centre Hospitalier Universitaire de Nancy, Nancy, France
[z] Service de neurochirurgie pédiatrique, Fondation Rothschild, Paris, France
[aa] CHU Grenoble Alpes, Neurology Department, Grenoble, France

ARTICLE INFO

Keywords:
Brain atlas
Epilepsy
Intracranial electroencephalogram
Cortico-cortical evoked potentials
Connectivity mapping

ABSTRACT

In patients with pharmaco-resistant focal epilepsies investigated with intracranial electroencephalography (iEEG), direct electrical stimulations of a cortical region induce cortico-cortical evoked potentials (CCEP) in distant cerebral cortex, which properties can be used to infer large scale brain connectivity. In 2013, we proposed a new probabilistic functional tractography methodology to study human brain connectivity. We have now been revisiting this method in the F-TRACT project (f-tract.eu) by developing a large multicenter CCEP database of several thousand stimulation runs performed in several hundred patients, and associated processing tools to create

* Corresponding author. Grenoble Institut des Neurosciences, Chemin Fortuné Ferrini, Bât EJ Safra, La Tronche, 38700, France.
E-mail address: Olivier.David@inserm.fr (O. David).

https://doi.org/10.1016/j.neuroimage.2018.07.039
Received 29 January 2018; Received in revised form 21 June 2018; Accepted 15 July 2018
Available online 17 July 2018

a probabilistic atlas of human cortico-cortical connections. Here, we wish to present a snapshot of the methods and data of F-TRACT using a pool of 213 epilepsy patients, all studied by stereo-encephalography with intracerebral depth electrodes. The CCEPs were processed using an automated pipeline with the following consecutive steps: detection of each stimulation run from stimulation artifacts in raw intracranial EEG (iEEG) files, bad channels detection with a machine learning approach, model-based stimulation artifact correction, robust averaging over stimulation pulses. Effective connectivity between the stimulated and recording areas is then inferred from the properties of the first CCEP component, *i.e.* onset and peak latency, amplitude, duration and integral of the significant part. Finally, group statistics of CCEP features are implemented for each brain parcel explored by iEEG electrodes. The localization (coordinates, white/gray matter relative positioning) of electrode contacts were obtained from imaging data (anatomical MRI or CT scans before and after electrodes implantation). The iEEG contacts were repositioned in different brain parcellations from the segmentation of patients' anatomical MRI or from templates in the MNI coordinate system. The F-TRACT database using the first pool of 213 patients provided connectivity probability values for 95% of possible intrahemispheric and 56% of interhemispheric connections and CCEP features for 78% of intrahemisheric and 14% of interhemispheric connections. In this report, we show some examples of anatomo-functional connectivity matrices, and associated directional maps. We also indicate how CCEP features, especially latencies, are related to spatial distances, and allow estimating the velocity distribution of neuronal signals at a large scale. Finally, we describe the impact on the estimated connectivity of the stimulation charge and of the contact localization according to the white or gray matter. The most relevant maps for the scientific community are available for download on f-tract. eu (David et al., 2017) and will be regularly updated during the following months with the addition of more data in the F-TRACT database. This will provide an unprecedented knowledge on the dynamical properties of large fiber tracts in human.

1. Introduction

Anatomical studies of the human brain connections, particularly from diffusion tensor imaging (DTI) data (Guevara et al., 2012), have described the brain as a highly connected network structured around modules connected by hubs (Hagmann et al., 2007; Sporns et al., 2005). This structural connectivity partly shapes the functional coupling between the different neuronal populations (Hagmann et al., 2008), which can be highlighted by correlating the activity of different brain areas using non-invasive neuroimaging, such as functional magnetic resonance imaging (fMRI), electroencephalography (EEG) or magnetoencephalography (MEG). By using in silico models of the brain, it is also possible to predict large scale neural dynamics from underlying anatomical connectivity (Deco et al., 2013). In this type of models, the directionality and propagation latencies along large fibers have a major impact on the generated dynamics (Petkoski et al., 2016). These parameters are only measurable in human through direct electrical stimulations (DES) applied on the cortex (David et al., 2013; Keller et al., 2014b).

Low frequency stimulations are performed in drug-resistant epileptic patients, commonly at 1 Hz or below, and called single-pulse electrical stimulations (SPES), with the brain signals go back to their baseline after each pulse (Valentín et al., 2002). The electrical stimulation is believed to depolarize a neuronal population around the stimulation site, which will transmit signals along cortico-cortical fibers and depolarize at distance several populations of neurons in other cortical areas (Keller et al., 2014b). This is a way to elicit signals resembling physiological propagation at the cortex level. The responses to a DES, recorded with cortical grids (electrocorticography, ECoG) or intracerebral depth electrodes (stereo-electroencephalography, SEEG), and averaged over a set of pulses, are called the cortico-cortical evoked potentials (CCEP). This single-pulse methodology has been used in a clinical routine in some epilepsy patients to infer epileptogenic areas (Kahane et al., 1993), to perform functional mapping of various networks, for instance language (Conner et al., 2011; Enatsu et al., 2013a; Koubeissi et al., 2012; Matsumoto et al., 2004) and motricity (Enatsu et al., 2013b; Kikuchi et al., 2012; Matsumoto et al., 2007), and to study intra- or inter-hemispheric connectivity within or between brain lobes (Catenoix et al., 2005; David et al., 2013; Krieg et al., 2017; Lacruz et al., 2007).

Connectivity studies from iEEG often suffer from a small spatial sampling available in a single patient, number and coverage of recording electrodes are limited and mainly focused on the epileptic network of interest. In addition, the connectivity estimated from CCEP depends on the stimulation parameters (Donos et al., 2016b), which largely differ between clinical epilepsy centers: for instance, current intensity between 0.5 and 4 mA is used for SEEG, and between 8 and 15 mA for ECoG, with pulse duration ranging from 1 to 3 ms and pulse shape can be biphasic or monophasic. A multicenter database in a large number of patients should help avoiding these two limitations when inferring the dynamical properties of a large number of possible cortico-cortical connections. So far, CCEP studies are limited regarding these two points as they involved only 1 or 2 centers and described small series of patients from 5 to 25 patients (Boido et al., 2014; Conner et al., 2011; Donos et al., 2016a; Entz et al., 2014; Keller et al., 2014a; Krieg et al., 2017; Matsumoto et al., 2007). Following our initial study aiming at going beyond these limitations with a probabilistic approach developed with a small dataset of 35 patients (David et al., 2013), we started a multicenter project (F-TRACT, f-tract. eu) aiming at developing a large CCEP database for describing the spatial-temporal properties of cortico-cortical connections at an unprecedented precision in humans.

The aim of this report is to present a snapshot of the methods and data of the F-TRACT project with an extended pool of 213 patients. The CCEPs were processed using an automated pipeline, and supervised at the end to control the data quality. We implemented group statistics of CCEP features for each brain parcel explored by iEEG electrodes. The most relevant maps for the scientific community are available for download on f-tract. eu (David et al., 2017) and will be regularly updated during the following months with the addition of more data in the F-TRACT database.

2. Materials and methods

2.1. Data acquisition

The F-TRACT project follows ethical guidelines for conducting international multicenter post-processing of clinical data as defined by the International Review Board at INSERM (protocol number: INSERM IRB 14–140). The F-TRACT database nowadays contain data coming from 792 SEEG explorations explored in 25 epilepsy centers (Paris La Pitié-Salpêtrière Hospital, Rennes University Hospital, Brno Epilepsy Center, Montreal Neurological Institute, Lyon Neurological Hospital, Marseille La Timone Hospital, Yuquan Hospital Epilepsy Center, Canton Sanjiu Brain Hospital Epilepsy Center, Paris Necker Hospital, Helsinki Hospital for Children and Adolescents, Paris Saint-Anne Hospital, Lille University Medical Center, Strasbourg University Hospital, Toulouse University Hospital, Barcelona Hospital del Mar, Bucharest University Emergency Hospital, Milan Niguarda Hospital, Nancy University Hospital, Paris

Rothschild Foundation, Valencia La Fe University Hospital Valencia, Rome Bambino Gesù Children's Hospital, London King's College Hospital, Freiburg Medical Center, Paris Bicêtre Hospital).

For this report, we used data from a subgroup of 217 SEEG evaluations performed in 213 epilepsy patients (108 females, 105 males; age at evaluation from 2 to 58 years old – mean age 22 ± 14) acquired in four centers (Grenoble University Hospital, Paris Rothschild Foundation, Nancy University Hospital, and Lyon Neurological Hospital). The seizure onset zone was clinically estimated in temporal lobe (left: n = 59; right: n = 45), frontal lobe (left: n = 36; right: n = 32), central region (left: n = 6; right n = 12), parietal lobe (left: n = 12; right: n = 17), occipital lobe (left: n = 13; right: n = 5) and insular cortex (left: n = 16; right: n = 22), with multilobar spread in 56 cases. The localization of the seizure onset zone was not explicitly modelled in this study (see Discussion). The patients gave their consent to undergo invasive recordings and low frequency stimulation as part of a pre-surgical evaluation of their drug-resistant epilepsy. In Grenoble, runs of 40 stimulations were performed at 1 Hz between two contiguous contacts in the gray matter, and sometimes in the white matter, using monophasic 1 ms duration pulses at 3 mA. Signals were acquired at 512 Hz or 1024 Hz (for more details about the standard clinical procedure, see (David et al., 2013)). The procedure was similar for the other centers, but biphasic pulses were used at Rothschild Foundation and in Nancy, and the stimulation intensity ranged from 1 to 4 mA.

2.2. Neuroanatomy

For each patient, a preoperative anatomical MRI (T1 contrast) and an image with SEEG electrodes (T1 MRI or CT scan) were obtained in order to position SEEG electrodes. The average number of recording bipolar contacts per patient was 149 ± 31. The electrode contacts were localized and anatomically labeled using the IntrAnat Electrodes software (Deman et al., 2018) compatible with the BrainVisa software (Rivière et al., 2009). Briefly, the volumetric images acquired before (pre, 3D T1 MRI) and after (post, 3D T1 MRI, T2 MRI or CT) the electrodes implantation were co-registered using a rigid-body transformation computed either by ANTs (Avants et al., 2011) or SPM12 (Ashburner, 2009) software. The gray and white matter volumes were segmented from the pre-implantation MRI using Morphologist as included in BrainVisa (http://brainvisa.info). The electrode contact positions were computed in the native and MNI referentials using the spatial normalization of SPM12 software. For each patient, cortical parcels were obtained for different anatomical atlases defined either in the MRI native space (MarsAtlas (Auzias et al., 2016)) or in the MNI space (Brodmann (1909), Automated Anatomical Labeling AAL (Tzourio-Mazoyer et al., 2002) and MaxProbMap (Hammers et al., 2003)). Each electrode contact was assigned to the gray or white matter and to specific anatomical parcels by taking the most frequent voxel label in a sphere of 3 mm radius around each contact center. In this study, we mainly describe results obtained with the MarsAtlas parcellation scheme, a surface-based method using the identification of sulci and a set of 41 regions of interest per hemisphere.

2.3. SEEG preprocessing

The SEEG signals were preprocessed automatically using a pipeline composed of the following steps, supervised at the end for data quality check: detection of each stimulation run from stimulation artifacts in raw iEEG files (*i.e.* a set a pulses consecutively applied between the same pair of contacts), bad channels detection with a machine learning approach (Tuyisenge et al., 2018), and stimulation artifact correction with a model-based method (Trebaul et al., 2016). Briefly, the stimulation artifacts were detected from fast transients in signals and adequate template matching between events to avoid the selection of stimulation-unrelated events. The detection of bad channels was based on a supervised machine-learning model trained on a learning database with channels already classified by experts and using a set of features quantifying the signal variance, spatio-temporal correlation and non-linear properties. The stimulation artifacts were removed on single-trials using a template matching method based on an electrical model of the electrical/tissue interface stable across stimulation and recording parameters (Trebaul et al., 2016), allowing us to consider the first milliseconds after stimulation for the CCEP analysis. At the end of the pre-processing, the SEEG signals were re-referenced with a local bipolar montage between adjacent contacts of the same electrode to increase the spatial specificity of the effects and the re-referenced signals were band-pass filtered between 1 and 45 Hz to best identify the CCEP components.

2.4. CCEP processing

CCEP were obtained using a robust-averaging method aiming at removing any possible spurious component due to non-stimulation triggered events, such as interictal epileptic spikes. Responses over pulses were averaged together, but excluding the trials showing a response energy 3 times higher than the median response energy over the whole stimulation run (David et al., 2013). After averaging, the CCEP on each channel was baseline-corrected, considering the baseline as the [−200 -10] ms interval before the pulse, and z-scored with respect to the same baseline. Z-scoring quantifies the signal-to-noise ratio on each channel, thereby allowing easy intra- and inter-patient statistics.

The absolute value of the z-scored CCEP (z-CCEP) was used to identify

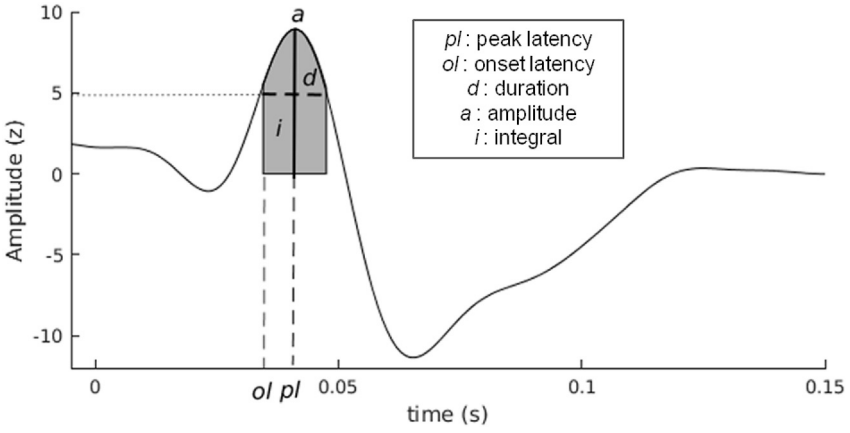

Fig. 1. Description of the features on a z-CCEP: onset and peak latencies, component duration, peak amplitude and component integral. The raw z-CCEP is shown on the figure but the features were computed over its absolute value.

the first significant component which was characterized by the following features (Fig. 1):

- *Onset latency*: latency of the first sample with an amplitude exceeding the significance threshold (e.g. 5 z);
- *Peak latency*: latency of the first peak above the significance threshold;
- *Duration*: first time window with consecutive samples exceeding the significance threshold. If the signal amplitude went down this threshold but stayed above a minimal threshold ($z = 4$) for less than 5 ms, this signal part was still considered as significant;
- *Integral*: signal integral computed over of the first significant time window;
- *Amplitude*: amplitude of the first peak above the significance threshold.

These features extract dynamical properties (onset and peak latencies, and duration) and strength (integral and amplitude) of the connections.

2.5. Group analyses at the ROI level

Given that long range structural brain connectivity is largely reproducible in healthy subjects (Guevara et al., 2012), similar spatio-temporal patterns of the first component of the CCEP can be assumed to be recorded for a given pair of stimulated and recorded regions of interest (ROI) between individuals. It is therefore possible to develop simple methods to infer ROI-specific maps for each CCEP feature over all stimulations when stimulating a particular ROI, providing a significant response is repetitively detected. For the results shown below, we considered $z = 5$ as the significance threshold for the z-CCEP amplitude and focused on the features of the first significant CCEP component. Different thresholds, from $z = 1$ to $z = 7$, were also explored to assess the influence of the z value on the group features.

The CCEP values from the electrode contacts were transferred to the brain parcels at the group level. According to the threshold of significance, each contact was declared as responsive or not using a binary variable (1 with a significant response during the first 200 ms; 0 with no significant response during the first 200 ms) and, when responsive, the CCEP features were stored. Then all the contacts in the database stimulated in a given ROI were used to estimate the group response from all the contacts corresponding to the same recording parcels: the CCEP features and binary responses for each contact were transferred at the parcel level by computing the median for the features and averaging the binary response for all the contacts belonging to the same parcel. The maps of connectivity probability for each stimulated ROI correspond to the averaged binary response. For the sake of robustness, we created group values only for parcels with at least 5 response values for a given stimulated ROI.

Putting together the data from all stimulations, we were able to produce connectivity matrices from the stimulated ROIs towards the recorded ROIs, as well as matrices of CCEP features, for every parcellation scheme available. The matrices for the different parcellation schemes were created with the same anatomical ordering: the first parcels corresponded to the left hemisphere and started from the occipital lobe to the insula, through the temporal, parietal, cingulate, frontal and orbito-frontal cortices. Within a lobe, we followed the principal gyri and tried to best ensure spatial continuity between the lobes. The second part of the matrices accounted for the right hemisphere, using the same order. Some regions (subcortical structures like the amygdala and hippocampus) were not present in some parcellations. The extensive list of parcels is presented in Table S1 of Supplementary data. Furthermore, assuming hemispheric symmetry, we computed the symmetrical CCEP matrix representing the average of the connectivity measures between the two hemispheres for the ipsi- and contra-lateral stimulation side. In case of no value for a parcel pair for one hemisphere, we kept the value from the other hemisphere in the symmetrical matrix. To compute symmetrical matrices for the number of available values, we simply added the numbers of each hemisphere.

The significance of the observed connectivity probability was obtained from surrogate distributions, which allow testing the null hypothesis that such connectivity probability values could be obtained without the stimulation. Surrogate data were generated with the following procedure: time series taken during the period before each stimulation run (baseline) were processed in exactly the same way as when computing CCEPs, but with stimulation events randomly distributed during baseline. Connectivity matrices surrogates were then obtained using the exact same number of random stimulation runs. Two hundred surrogate connectivity probability matrices were generated, allowing obtaining of the null distribution of connectivity probability for each parcel pair. The p value of the measured connectivity probability was then obtained for each parcel by comparing the measured value to the surrogate distribution.

The group analyses can be performed on any variable of interest. For example, we compared CCEP patterns in response to the stimulation of the white or gray matter, *i.e.* considering only stimulation contacts labeled in the white matter or only in the gray matter, respectively. We also looked at the effect of the input charge level on the inferred connectivity at the group level. To do so, charge levels were defined as the product of stimulation intensity (mA) and pulse duration (ms) (Donos et al., 2016b). According to the same study, the injected charge was responsible for most of the variations observed in connectivity results, independently of the stimulation mode. Four charge levels were predominant in our data, corresponding to ranges of 1, 2, 3 and 4 μC, ±0.250 μC. They will be referred to as the charge levels 1, 2, 3 and 4. We compared level 1 to the levels 2, 3 and 4 to analyze the change in probability when increasing the charge level and selected the same parcels pairs for the 3 comparisons. In order to best compare each level with the first one, the same patients were considered on each parcels pair and only stimulations in the gray matter were used. In total, 50 patients were used to compare level 1 with level 2, 54 for the comparison with level 3 and 43 with level 4. No threshold was used for the number of values needed to provide a probability value between each parcel pair.

2.6. Measurement of distance and conduction velocity between electrode contacts

We computed a measure of distance between the stimulating contact and the recording contacts that used the anatomical fibers which can be reconstructed from diffusion tensor imaging (DTI). Because the F-TRACT database does not contain any DTI information, those fibers were obtained from the ARCHI database built from 81 healthy subjects at the Neurospin center (Guevara et al., 2012). The fibers were described as sets of points repositioned in the MNI coordinate system after normalization of the anatomy of each subject. The distance between two contacts of each F-TRACT subject was defined as the distance averaged between subjects of the ARCHI database. This distance was defined as the length averaged over all fibers that were close enough to both contacts. In this study, only fibers that had a point at a distance below 1 cm from both contacts were used. In addition, the distance between parcels of each atlas was defined as the average distance between contacts belonging to the parcels. Finally, the matrix of conduction velocity was computed as the ratio between the distance and the onset latency matrix.

3. Results

3.1. Sampling matrices

The data taken from the 217 implantations processed here include 10 850 stimulation runs, *i.e.* on average 50 stimulation runs per implantation session. Because electrodes were placed for clinical reasons, their spatial distributions were heterogeneous, with a high density of contacts within the temporal lobe, between the temporal and the occipital lobes, and between the sensory-motor and temporal, parietal or frontal areas. Implantations were also usually sampling only one hemisphere and, hence,

much less contacts recorded inter-hemispheric responses, except for the temporal cortex that was frequently explored bilaterally. The spatial distribution of the contacts recording significant responses, from which CCEP features were computed, indicates high connectivity density within and between the somatosensory and motor areas as well as within the temporal cortex (Fig. 2C). For the majority of intra-hemispheric recordings, data were coming from several thousand implantations (Fig. 2B).

3.2. Connectivity probability

3.2.1. General description

The connectivity probability matrix, derived with threshold $z = 5$, was filled (as defined by at least 5 responses per parcel pair) for 96% of intrahemispheric connections and for 56% of inter-hemispheric connections (symmetrical matrix: Fig. 3B). One can observe high connectivity probability values and p values < 0.005 (Fig. 3C) within the rostro-frontal and orbito-frontal parcels. The value distribution was sparser between the other regions, although one can observe clusters composed of temporal and occipital parcels. In general, very few of inter-hemispheric values were significant, except for homologous parcels. The connectivity pattern between the two hemispheres was overall similar (Fig. 3A). We identified significant connections ($p < 0.005$) between 25% of the pairs for which a probability connectivity value was inferred, or 19% of all parcel pairs. The ith column of the connectivity

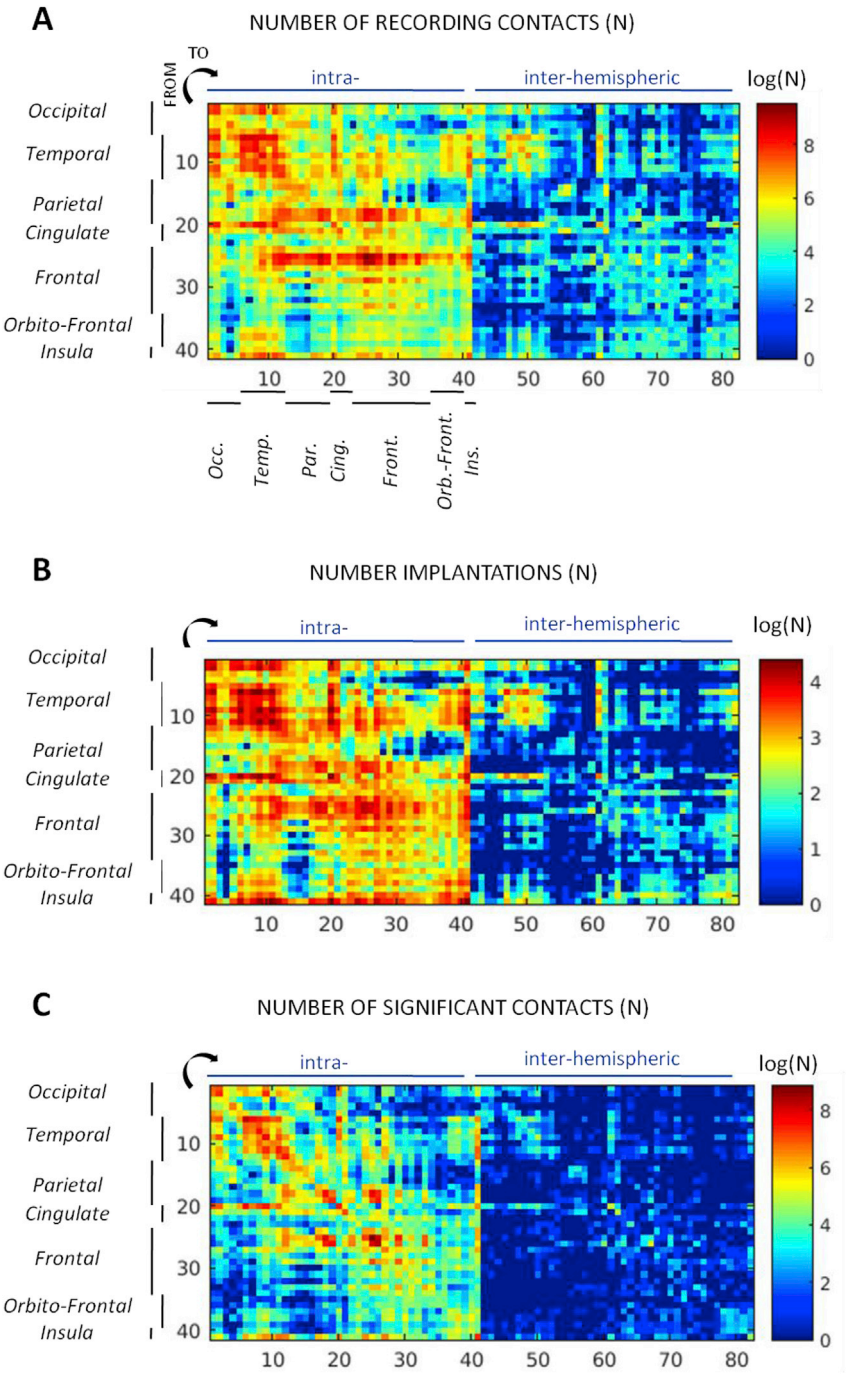

Fig. 2. Spatial log-distribution of the number of recording contacts (A), of contacts showing a significant CCEP (B) and of the number of implantations used for each parcels pair (C) for the MarsAtlas parcellation. The parcels were clustered by lobe and the values merged between the two hemispheres. A logarithmic scale was used for allowing distinguishing the large sampling differences between parcels.

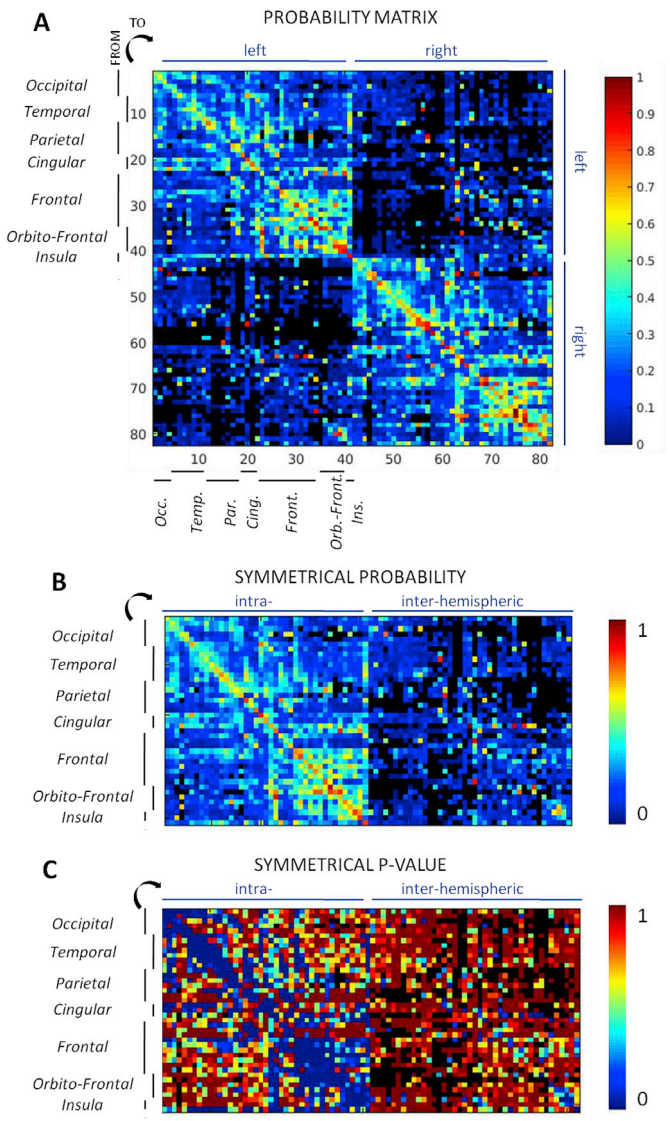

Fig. 3. (A) Connectivity probability matrix for the MarsAtlas parcellation. The black color corresponds to parcels pair with no data., (B) the symmetrical connectivity probability with merged values across hemispheres and (C) the symmetrical p-value matrix (minimum of 0.005).

matrix corresponds to the spatial pattern of response to the stimulation of the ith ROI of the parcellation scheme. For example, the map of the insula (Fig. 4A) shows the highest probability values within the stimulation parcel and then around the stimulation site toward the superior temporal, inferior parietal and frontal, the cingulate cortices and the homotopic parcels. Those were also the significant connections (Fig. 4B). The dataset containing the connectivity maps of the other areas of the MarsAtlas, Brodmann, AAL and MaxProbMap parcellation schemes is available for download (David et al., 2017).

3.2.2. *Effect of response detection threshold*

In order to test the impact of the threshold on the z-score of CCEP amplitude on the group results, we computed the connectivity probability matrices for different thresholds on z, from 1 to 7 with a step of 1. We found a high correlation coefficient between the matrices computed for a threshold of at least 3 (Fig. 5A and C). The threshold of significance at $p < 0.005$ determined from surrogates was negatively correlated to the z threshold used to compute the connectivity matrix (Fig. 5B and D). We found that a threshold at 5 provides the best trade-off between a centered distribution range, with a mean of 0.46 ± 0.16, and the most homogeneous repartition between its minimum and maximum for the connectivity probability values. We will keep this threshold for the rest of our analysis. Plotting the distribution of significant and non-significant connections made it clear that most of non-significant connections were longer than 50 mm (Fig. 5E).

3.2.3. *Effect of distance and charge levels*

The matrix of distance was computed by taking the averaged fibers distance between all pairs of contacts belonging to each pair of parcels (Fig. 6A). We found that the connectivity probability decreased with the distance, as demonstrated by the strong negative value (−0.62) of Spearman's correlation coefficient between the distance matrix (Fig. 6A) and the connectivity probability matrix (Fig. 3A). On average, a decrease was also observed in the connectivity probability values from 0.8 to less than 0.2 when the distance range increases (Fig. 6B, black line).

We analyzed connectivity matrices computed for different charge levels and compared the charge levels 2, 3 and 4 to the level 1. Different patients were available for the three comparisons but the same couples of parcels were selected for each one: we found 391 joint parcel pairs, distributed in the somatosensory, motor, cingulate, prefrontal and insular cortices. The difference between the mean probability obtained for the level 1 and on corresponding data in the same patients for levels 2, 3 and 4 as a function of distance (averages computed over 5 mm ranges) is shown on Fig. 6B as the surface between the two mean probability curves. The mean probability decreased in a similar way as for all the data together (black line). On average, the mean probability difference with the charge level 1 was larger for the highest charge levels: for charge level 2, the difference is 0.24 at distance = 15 mm and 0.07 at distance = 40 mm; for charge level 3, 0.36 and 0.21 for the same distances and for charge level 4, 0.33 and 0.21 for the same distances. In Fig. 5, we showed that connections with a probability below 0.2 are not likely to be significant. For the charge level 1, we now see that for a distance higher than 20 mm (averaged for the comparison with the 3 other levels) connections probabilities did not exceed 0.2 on average. In comparison, the mean probability remained higher than 0.2 for a distance of almost 30 mm (charge level 2), around 50 mm for charge levels 3 and 60 mm for level 4. It suggests that responses between 30 mm and 60 mm could be significant for high but not for low charge levels and responses recorded less than 20 mm away from stimulation were more likely to be significant for any charge injected.

3.2.4. *White vs. gray matter stimulation*

We computed the connectivity probability matrices comparing the stimulations performed in the white and gray matter (Fig. 7). On average, the connectivity probability was higher for the white matter (0.29) than for the gray matter (0.18) stimulations. This effect was stronger for short fibers as the difference of connectivity probability between parcels stimulated in white and gray matter was on average 0.16 for distances less than 30 mm and 0.05 for distances above 60 mm.

3.2.5. *Parcellation schemes*

All the group analyses were performed for 4 different parcellation schemes (MarsAtlas, Brodmann, AAL, MaxProbMap) to prepare the future utilization of the F-TRACT atlas by the neuroimaging community. Here we show the connectivity probability maps of the 4 different schemes, which looked similar because the spatial scales are on the same order (Fig. 8). The correspondence between atlases is available as supplementary data (Table S1). Other parcellation schemes will be added in the near future, in particular to reach finer spatial resolutions as provided by the Lausanne atlas (Hagmann et al., 2008).

3.3. *CCEP features*

3.3.1. *General description*

We provide here CCEP features values for around 75% (73% for the left and 78% for the right hemisphere) of intra-hemispheric and 44% of

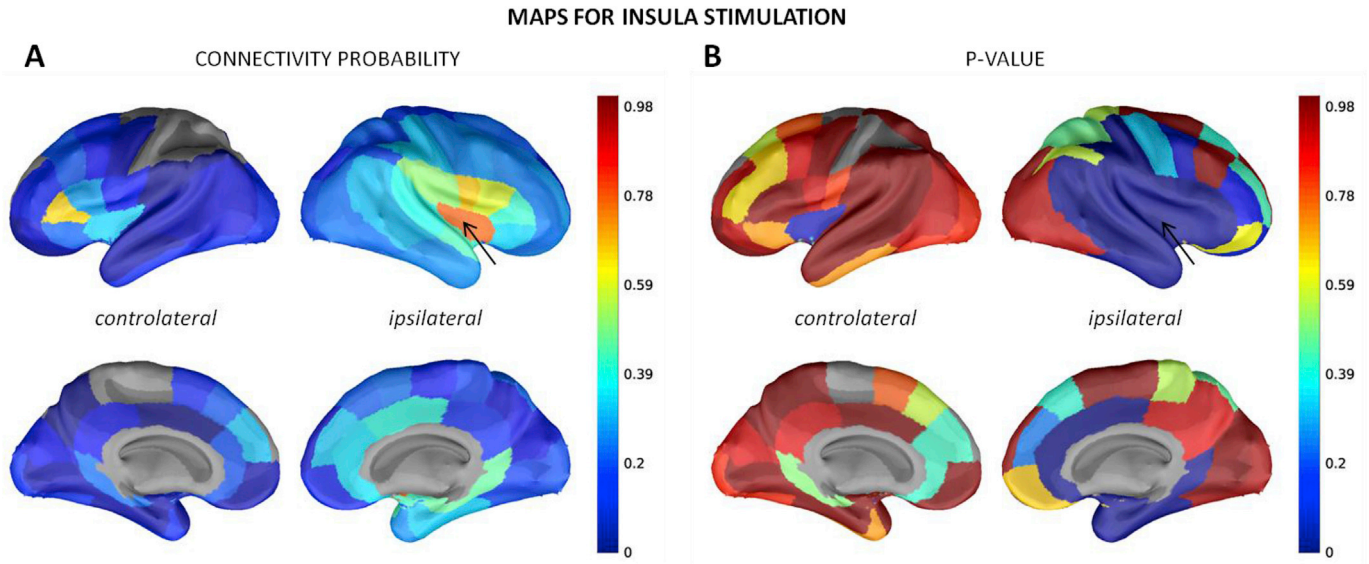

Fig. 4. Maps of connectivity probability (A) and the associated p-value (B) for the stimulation of the insula (black arrow).

the overall connections, and 67% of the possible connections (for which the probability value exceeded 0) for the MarsAtlas parcellation.

The closest parcels (near the matrix diagonal) had the smallest onset latency value (Fig. 9A). Most values were below 150 ms, with a peak in the distribution around 15–20 ms (Fig. 9B). We observed the same pattern but delayed (mean: 8 ms) for the peak latency (Fig. 9C). The peak in the distribution of peak latency at around 20 ms was more predominant than for the onset latency (Fig. 9D). The velocity values, derived from the distance and the peak latency, ranged mainly between 0.2 and 6.0 m/s, with a peak around 1 m/s (Fig. 9F). The highest values were found for inter-hemispheric connections (Fig. 9E). The duration values ranged mainly between 5 and 25 ms, with a peak around 15 ms (Fig. 9G and H). The first component integral was strongest between occipital and temporal parcels, as well as within rostro- and orbito-frontal ones (Fig. 9I) with values usually between 10 and 200 z^2 (Fig. 9J). Finally, the amplitude matrix revealed similar connectivity patterns as the probability matrix (Figs. 9K and 3A, Spearman's correlation coefficient = 0.62, $p < 0.001$) with most values remaining below 10 z (Figure 9L).

3.3.2. *Effect of distance*

We studied the effect of distance on all the features, except the velocity since it was computed from the distance matrix itself. In general, the signals propagated first and with a higher strength around the stimulation site, the homologous areas and then to more distant regions (Fig. 10C). The distance correlated with both latencies: Spearman's correlation coefficient rho between the distance (Fig. 4A) and the onset and peak latency matrices was 0.44 and 0.42 ($p < 0.001$), respectively. We observed an increased mean value of latency when increasing the distance range from 20 ms for the closest parcels pairs to around 70 ms for those more far apart (Fig. 10A). The duration of the first CCEP component was independent from distance (rho = 10^{-5}, p = 0.99). But, similarly to the correlation with connectivity probability (Fig. 5), strength features negatively correlated with the distance: rho = −0.50 with the amplitude and −0.15 with the integral (p-values < 0.001 for both). On average, the response amplitude decreased from 9.5 to 7 z from 1–2 to 9–10 cm and the integral ranges from 85 to 70 z^2 (Fig. 10B).

3.3.3. *Feature maps*

Using the insula as an example, we show in Fig. 11 the features maps that are computed for the stimulation of each ROI, obtained when both hemispheres are merged together. The same maps for the other ROIs are available as a public dataset in (David et al., 2017). The latency maps (onset and peak latencies: Fig. 11A and B) showed first the CCEP propagation first all around the stimulated parcel (insula), reaching the ipsilateral superior temporal, inferior parietal and frontal parcels. Then, the response propagates towards the contralateral middle temporal and medial frontal areas, the ipsilateral cingulate cortex, and the more distant frontal, orbito-frontal and superior parietal parcels. Finally, CCEP components are observed in several distant contralateral parcels but not significantly (Fig. 4B). Onset and peak latencies are similar but with an offset of around 10 ms. Latencies and velocity values are smaller for close ipsilateral parcels and homologous areas (Fig. 11C). In very close parcels, homologous areas and also more distant regions like the ipsilateral orbito-frontal cortex, the response remained longer above the significance threshold (Fig. 11D). In addition, the strength (amplitude and integral: Fig. 11E and F) of close ipsilateral and homotopic parcels is higher than for other regions.

4. Discussion

In this study, we characterized maps of connectivity probability and of CCEP features representing biophysical properties of the tracts, and provided an unprecedented knowledge on the dynamical properties of large fiber tracts in human. We presented the methods used for the first release of the F-TRACT functional tractography atlas (f-tract.eu) that brings new dynamical information on the cortical effective connectivity. We developed maps of connectivity probability and of CCEP features representing biophysical properties of the tracts. We also tackled several caveats in the CCEP study methodology previously highlighted in (Keller et al., 2014b) by including early responses in the CCEP analysis and studied in a large population of subjects. We provided connectivity maps of the whole cortex and symmetrical maps merged between the two hemispheres and for different parcellations, so they could easily be compared and used in the scientific community. Finally, the large amount of data, although heterogeneous from a methodological point of view, allowed us to study the influence of different parameters of interest on connectivity such as stimulation charge and site.

4.1. *Methodological comments*

Our current processing pipeline includes novel methodologies that allow the processing of data acquired in multiple medical centers. Electrical stimulations performed with variable parameters induced different shapes of artifacts, that can be reduced by alternating the pulse polarity

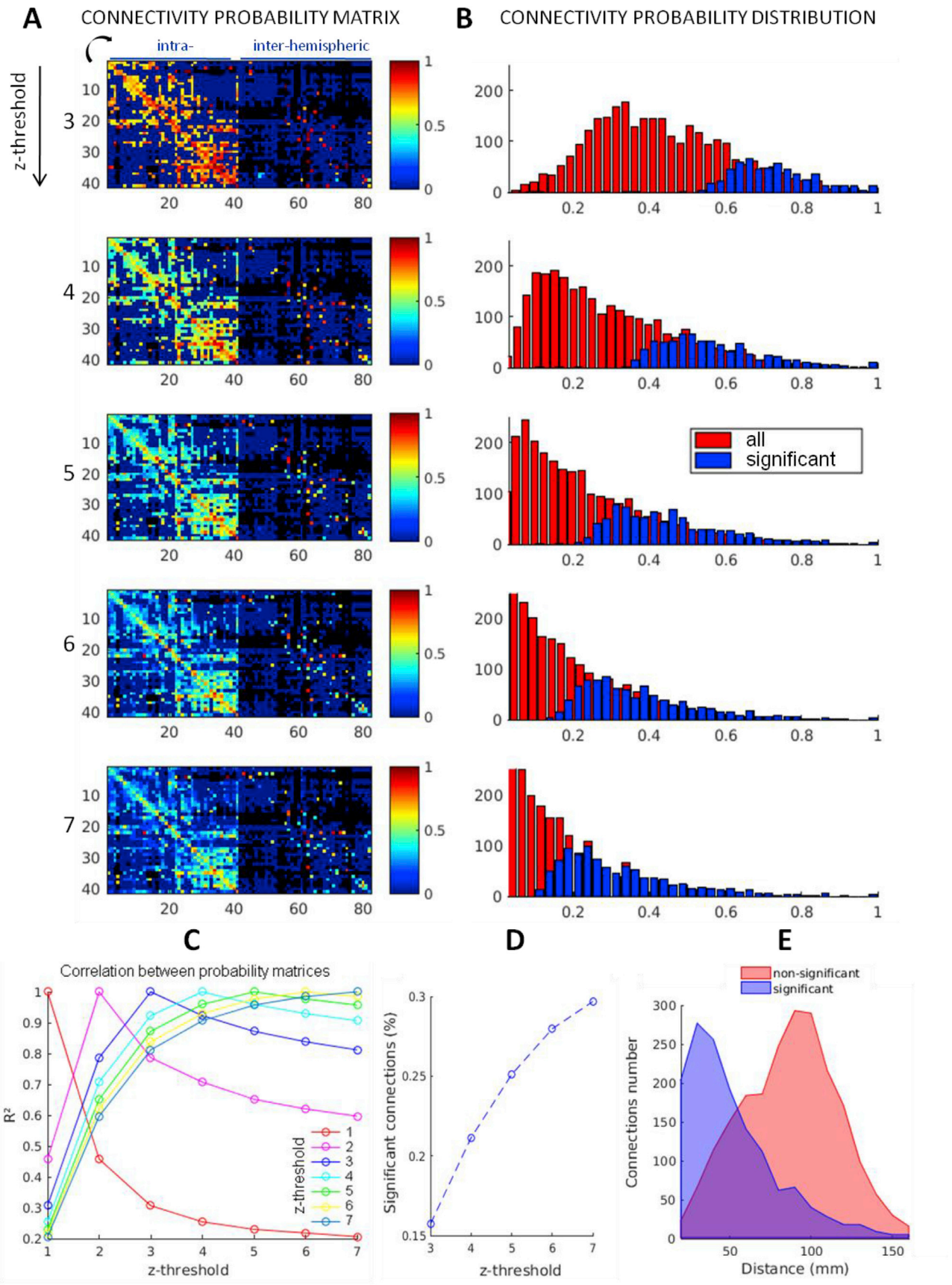

Fig. 5. (A) Connectivity probability matrices for different z thresholds, showing only significant connections ($p < 0.005$). (B) Distributions of the connectivity probability (all and only significant connections). (C) Correlation coefficients between probability matrices pairs computed for different z thresholds. (D) Number of significant connections for the different thresholds. (E) Number of connections as a function of the distance.

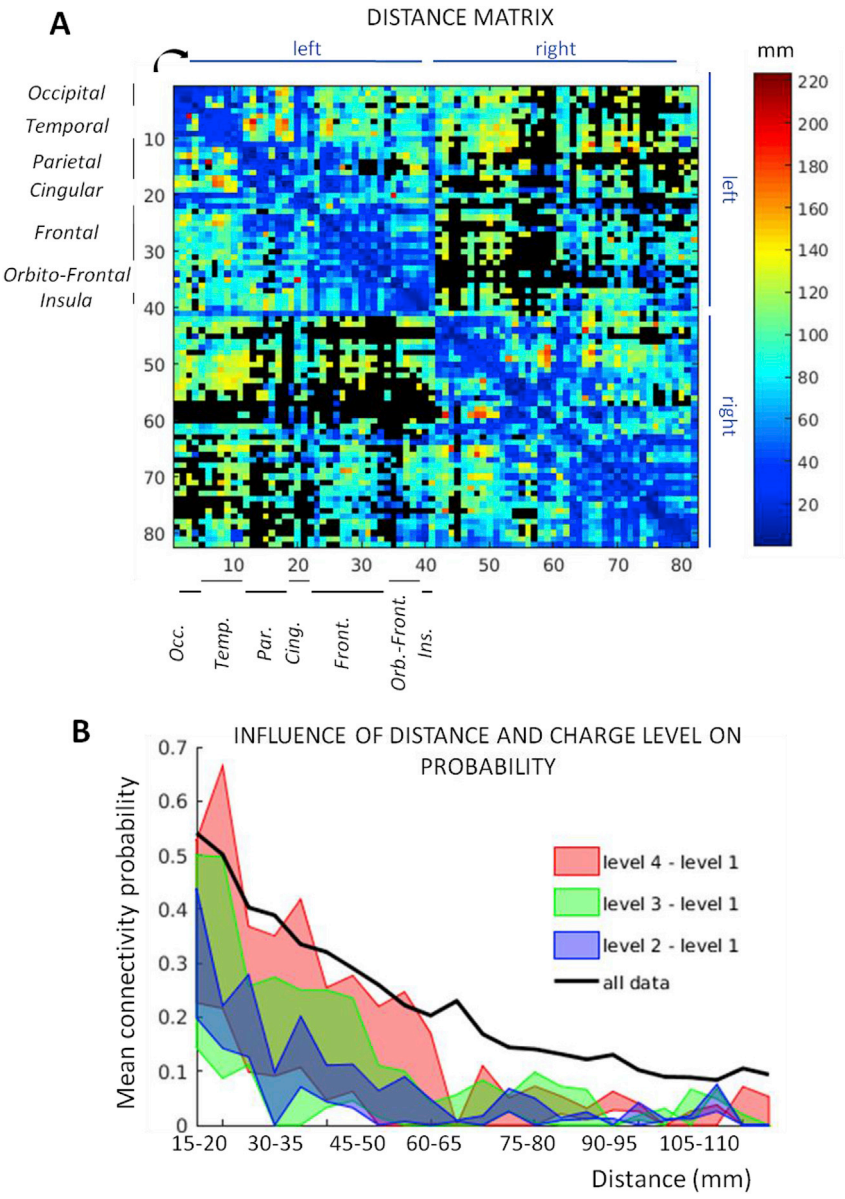

Fig. 6. (A) Fibers distance matrix between all recorded parcels pairs. (B) Mean connectivity probability as a function of distance (black line) and charge levels: colored surfaces correspond to the difference of the mean probability between higher charge levels (2: blue, 3: red, 4: green) and charge level 1, on the same patients and for the same parcels.

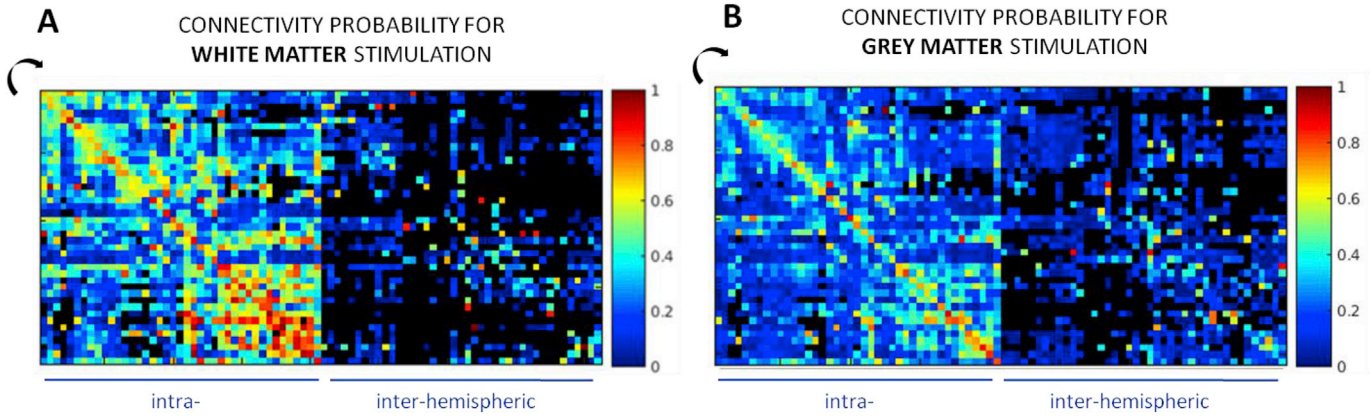

Fig. 7. Connectivity probability matrices for stimulations performed in the white (A) and the gray (B) matter. The effect of distance is reflected by higher values in the white matter for parcels pairs close to the diagonal.

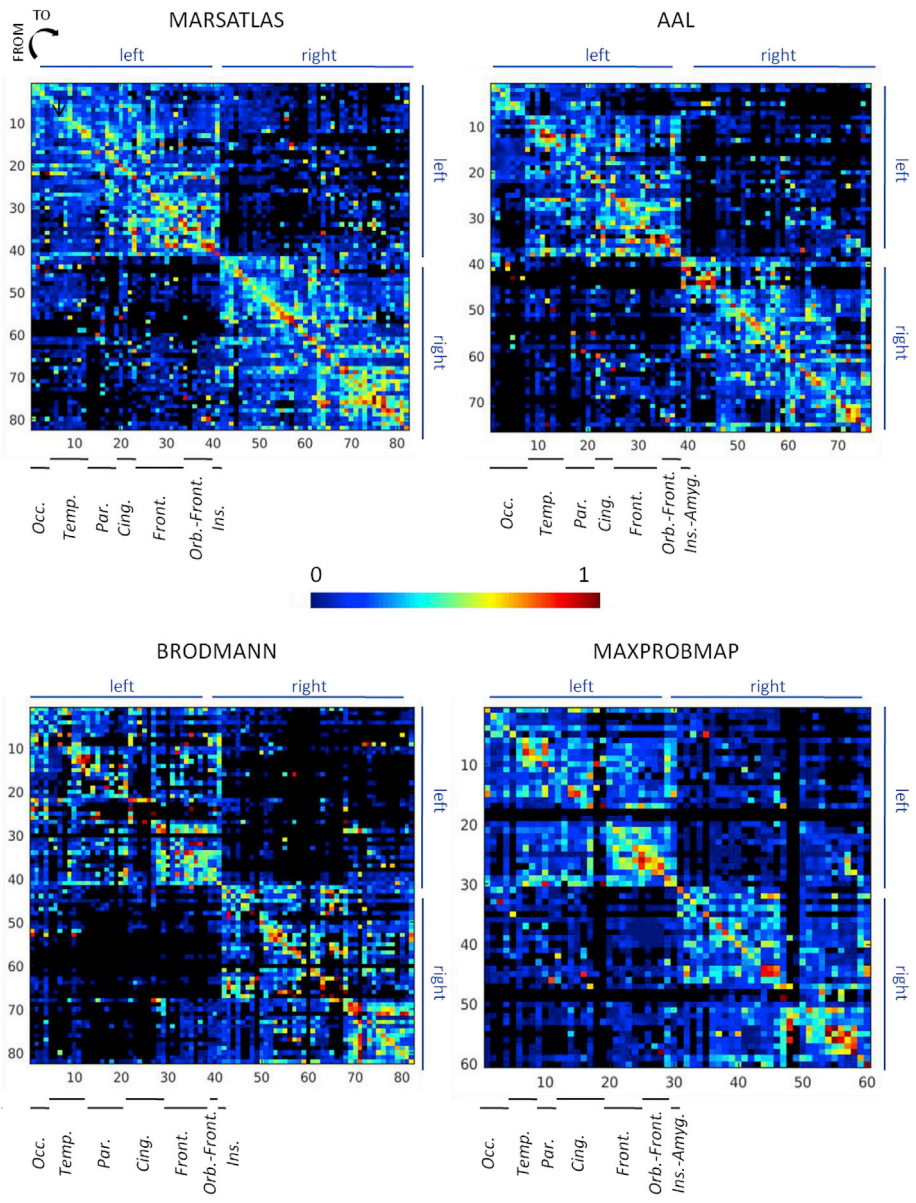

Fig. 8. Connectivity probability matrices for different parcellations ordered in a similar way.

when stimulating (Matsumoto et al., 2004). Alternatively, the first 5–20 ms after stimulation can be ignored during the CCEP analysis (Entz et al., 2014; Iwasaki et al., 2010; Kubota et al., 2013; Matsumoto et al., 2004). In our multicenter study, because we could not control the acquisition protocols, we developed a model-based correction method (Trebaul et al., 2016) that considers potential pulse differences across the different centers. By this mean, we included in our analysis early responses, likely to occur within the first milliseconds after stimulation. An automated detection method of bad channels (Tuyisenge et al., 2018) has also been developed to preprocess the data more efficiently.

For CCEP quantification, two kinds of approaches are currently used to identify the response components. They can be defined from visual analysis and described as two peaks (N1 and N2) distinguishable from baseline (Matsumoto et al., 2004). More recently, statistical tests (Almashaikhi et al., 2014; David et al., 2013) have been proposed to extract the significant responses. The baseline normalization and the use of a threshold on the z-score were chosen here because it allows intra- and inter-patient comparisons. Similar studies using z-score to assess the response significance used a threshold ranging between 2 and 6 standard deviations (Entz et al., 2014; Keller et al., 2011; Rosenberg et al., 2009). It was proposed that the value of $z = 6$ would guarantee the best sensibility/specificity ratio (Entz et al., 2014). Although the connectivity probability pattern remained similar for $z > 3$, we found that $z = 5$ guaranteed the most centered distribution (with a mean close to 0.5 and a range of values between 0.2 and 1). With that threshold, 25% of the connections with a connectivity probability above 0 were found significant after surrogates testing.

At the group level, we chose to pool together all the data and not to process them separately for the different patients. Although using z-scores allows the reduction of the inter-subject variability, there is still a 'patient effect' in the data that is not modeled explicitly. Modeling the inter-subject variability was extremely difficult in this study because our database is constituted of a large number of spatially incomplete and different datasets, as the brain of each patient was only very partially explored due to the limited spatial sampling and with stimulation protocols that differed between centers and patients. Therefore, we opted for a simple approach for our group analyses, considering the mean for connectivity probability and the group median value for all CCEP features to limit the potential influence of outliers. As the F-TRACT database evolves, we expect that the median values of the CCEP feature

distribution will converge to robust estimates. For this report, taking the mean or the median of all values between parcels pair without modeling the inter-subject diversity allowed us to maximize the cortex coverage with 217 implantations. We realize, however, that our results were likely biased by patients who underwent a large number of stimulations runs, e.g. 100 stimulations runs *vs.* 10 in other patients.

We developed a probabilistic approach for group analyses because there are many individual variabilities to be expected due to factors of different sorts: instrumental (e.g. stimulation parameters, electrode geometry, implantation schemes), physiological (e.g. age, gender, white and grey matter differences, functional specialization) and pathological (e.g. synaptic reorganization following lesion and/or epileptogenesis, medication). These factors cannot be controlled in an open and retrospective study as ours, but one can make inferences on them. The scientific objective of this report was to illustrate how instrumental factors influence connectivity estimates from CCEP data: we showed the effect of injected charge, of the gray vs. white matter stimulation, and of the distance between electrodes. More work is needed regarding the physiological and pathological factors.

In the future, the methodology will thus be improved by taking into account the epileptogenic areas and the patients' age, which are potentially two important confounds that must be addressed in dedicated studies. Currently, the CCEP literature is scarce on the effects of epileptogenic regions on CCEP spatio-temporal patterns. Overall it indicates that although epileptogenic cortices show larger CCEP amplitudes (Enatsu et al., 2012b; Iwasaki et al., 2010), with potentially larger bi-directionality of connectivity (Boido et al., 2014), the network topology may be preserved between normal and epileptic cortices (Keller et al., 2014a; Lacruz et al., 2007). Because these results were obtained with very small cohorts (less than 15 patients, except for (Lacruz et al., 2007) where 51 patients were used), this important question will need to be revisited. In the ramp-up phase of the generation of the F-TRACT atlas where it is important to maximize the number of estimated connections to start getting a picture for the whole brain, we chose to include all electrode contacts devoid of any artefact, whether or not they were susceptible to sample an epileptic network. To improve the physiological value of the forthcoming releases of the F-TRACT atlas by modeling explicitly the impact of epilepsy in connectivity estimates, which are potentially not limited to epileptogenic regions (Besson et al., 2017), we are now working on a new approach that aims at distinguishing physiological CCEP patterns from pathological ones. In addition, with a much higher number of patients processed in our database than for this report, we should be able to generate the F-TRACT atlas for different age ranges in order to avoid the age confound and to evaluate CCEP data can bring relevant information of brain maturation. It is again ongoing work.

In contrast to the approach we initially proposed (David et al., 2013), we chose here to cluster our data into parcels defined anatomically by 4 different atlases, and not to confine ourselves to the 3D MNI positions that can be ambiguous for inter-patient matching. The MarsAtlas parcellation (Auzias et al., 2016) was used as the main reference. This atlas transforms the cortical volume into a surface before defining the parcels in the patient space according to the detection of sulci. We believe that compared to a voxel-to-voxel approach to define the ROIs, the MarsAtlas approach can better cope with the inter-individual variability. Other parcellations allow the computation of connectivity results on other areas like the amygdala, and describe the different lobes with a variable number of parcels, notably: Brodmann and MaxProbMap schemes divide the cingular cortex into more parcels, whereas the AAL scheme more precisely describes the occipital cortex.

4.2. Characterizing the CCEP

The first CCEP peak likely represents direct connections (Matsumoto et al., 2004), and is commonly used to infer connectivity: its presence, latency or amplitude give complementary information about the connection significance, timing and strength. Its amplitude was shown to vary depending on the localization, greater around the stimulation sites (Enatsu et al., 2012a; Iwasaki et al., 2010), and significantly decreases with the fibers distance (Entz et al., 2014). Our results confirmed these findings. The amplitude also generally increases with the injected charge per pulse (Donos et al., 2016b), which is in correspondence with our results on connectivity probability at the parcel level. The same study also mentioned the variability of the latency depending on the stimulation parameters, but this has not been quantified yet in our framework. Although a lot of studies chose to rely only on the response strength (its integral over a fixed time window), and mainly on the amplitude parameter (Boido et al., 2014; Enatsu et al., 2013a, 2015; Kubota et al., 2013), we considered that the timing information adds a dimension to the representation of brain interactions that cannot be estimated using common functional connectivity measures. We thus chose to explore simultaneously both dynamical and strength related CCEP characteristics.

The peak around 20 ms in the peak latencies distribution (the median of all values recorded between each parcel pair) showed the importance of including early responses in the analysis. Depending on the localization and relative distance between stimulation and recording contacts, the latency range varied a lot: an average of 4.6 ms between the fornix and the hippocampus (Lacuey et al., 2015), from 48.2 to 122.0 ms between the basal bilateral temporal regions (Umeoka et al., 2009), a large range of 9–199 ms between different cortex areas (Enatsu et al., 2012a). Our results showed indeed an effect of distance on the latency values at the cortex level that can be attributed, at least partially, to the conduction time through the fibers. This corroborates the idea that, although our latency measures include synaptic integration in the stimulated and recording areas, the velocity we infer by using the fibers distance can reflect an actual conduction velocity. The conduction velocity values we found (peak distribution around 1 m/s) were comparable with those reported in before, between 0.88 and 3.64 m/s in human (Wilson et al., 1990) and in animals (Swadlow, 1989).

4.3. Effect of distance

The decrease of connectivity probability with the distance should not be attributed only to a loss of charge. Indeed, several studies have highlighted the high density of local anatomical connections as a way for the brain to minimize wire length (Ercsey-Ravasz et al., 2013; Markov et al., 2013). The small world configuration facilitates local interactions and allows remote connections through hub regions (Sporns et al., 2005). In our data, the analysis of significant connections mainly removed long-range connections, meaning that these, if existent, are not reproducible enough across patients to be distinguished from noise. However, we could still observe significant connections up to 11 cm away from the stimulation parcel, which can partly be attributed to inter-hemispheric homotopic connections.

4.4. Effect of charge

We showed that different charge levels, defined as the product of pulse intensity and its duration, induced different response patterns. Higher charge levels activated more connections, usually more distant from the stimulation site. Networks activated for a low charge level were also usually included in the networks activated for a high charge level. As a result, the connectivity probability values generally increased with charge levels. We also quantified the distance scale of connections easily activated (below 2.0 cm), as opposed to connections less likely to be activated (more than 4.0 cm). Including values corresponding to different charge levels in the same atlas adds to the overall statistical power. It also tends to lower probability values for parcels pairs for which we have more data acquired by injecting less charge. Especially for those connections with a fiber distance between stimulation and recording parcels around 3.0–5.0 cm and that could be reachable with higher pulse intensities. We suggest that electrical stimulations applied with SEEG

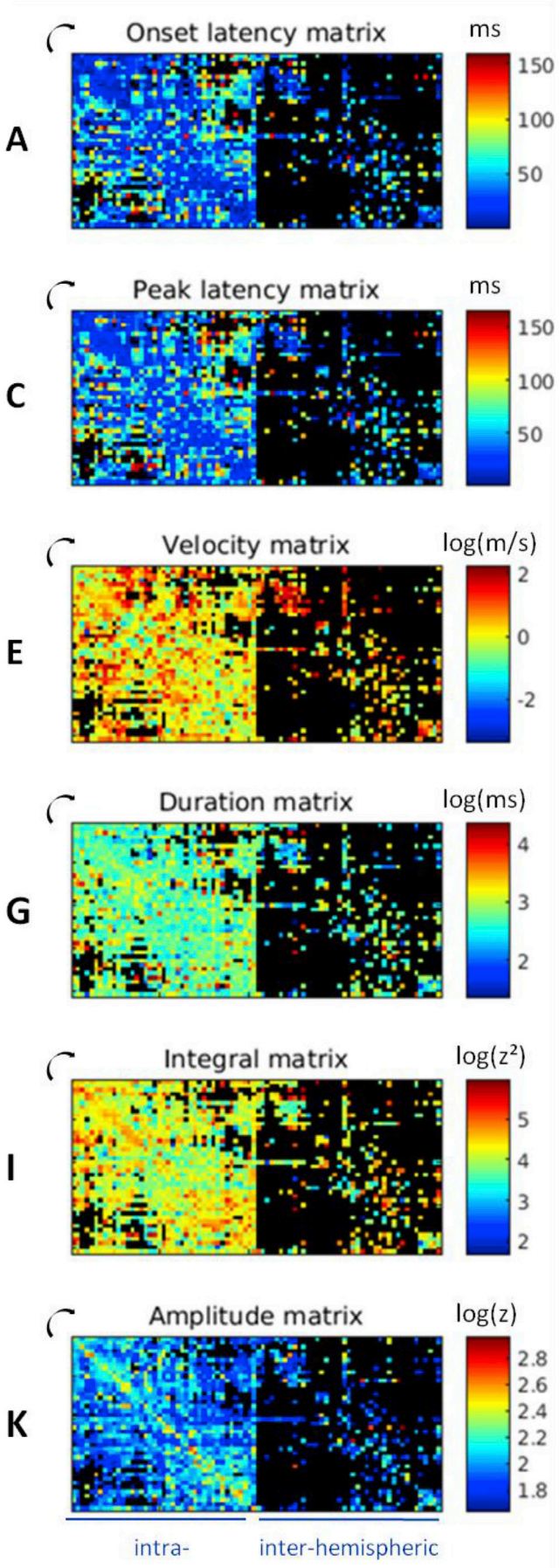

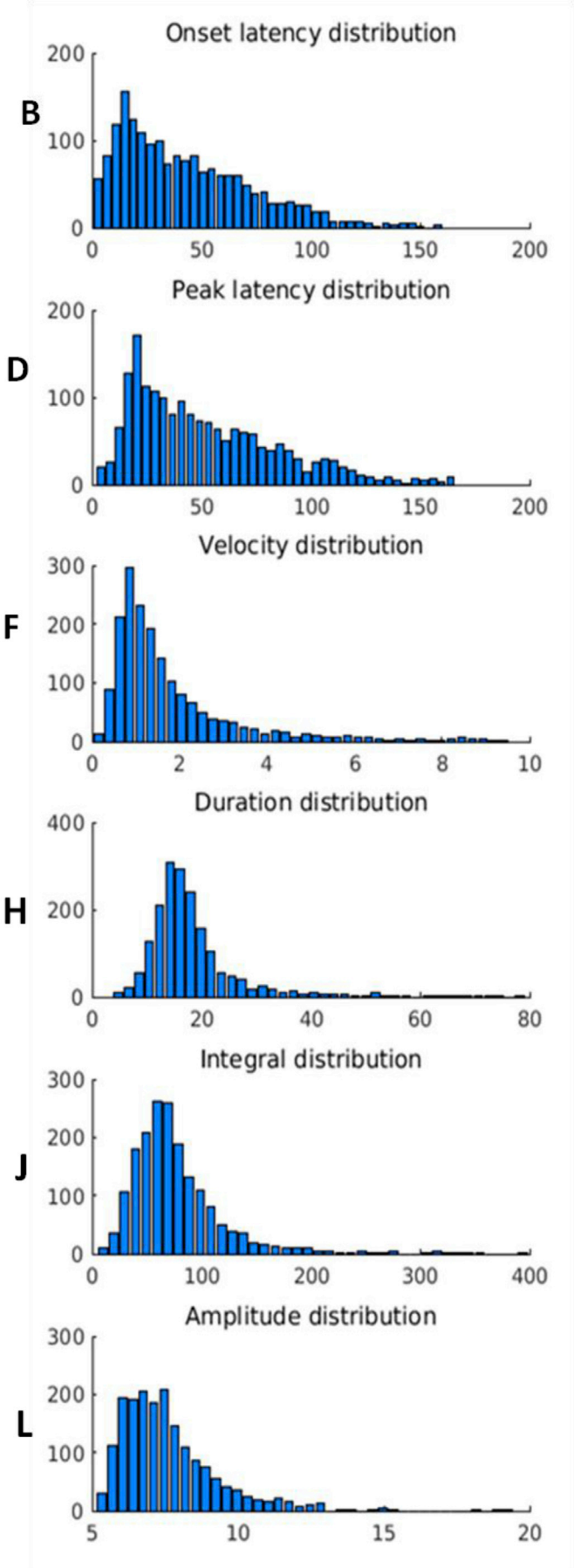

(caption on next page)

Fig. 9. Matrices of the features and their distribution between parcels for the MarsAtlas parcellation: (A) onset latency matrix, (B) onset latency distribution, (C) peak latency matrix, (D) peak latency distribution, (E) velocity matrix, (F) velocity distribution, (G) duration matrix, (H) duration distribution, (I) integral matrix, (J) integral distribution, (K) amplitude matrix, (L) amplitude distribution. For the velocity, the duration, the integral and the amplitude, a log scale was used and outliers (with values above the maximum displayed) have been removed to best display the overall data: they account respectively for 0.9%, 0.3%, 0.3% and 0.1% of the values.

methodology and aiming at inferring connectivity should be performed with a product of pulse intensity and duration exceeding 1 μC because they are more likely to activate cell bodies at the stimulation site (Ranck, 1975). In our experience, they are more likely to lead to larger brain networks activations and to reveal more functional connectivity information.

4.5. CCEP generation and stimulation in the white or gray matter

Although CCEP studies generally consider only gray matter stimulations, stimulations in the white matter have also been performed, showing that the sum of subcortico-cortical evoked potentials (SCEP) latencies between two cortical areas is close to the CCEP latency between the same regions (Yamao et al., 2014). Axono-cortical evoked potentials with similar responses recorded in the gray matter and small latencies (between 11.0 and 14.8 ms) have also been described (Mandonnet et al., 2016).

A commonly accepted hypothesis about CCEP generation mechanisms states that the electrical stimulation activates mostly pyramidal cells, directly or indirectly through inter-neurons (Matsumoto et al., 2004). The signal then propagates mainly orthodromically, but without excluding antidromic propagation, through white matter fibers (Yamao et al., 2014) toward the projection site where the pyramidal cells are also activated (Keller et al., 2011). White matter stimulation could activate the fibers directly, which makes the orthodromic propagation more unlikely and enhances the probability of antidromic activation. Our results showed an increase of connectivity probability for white matter stimulation on average on the whole matrix but especially between the closest neighboring areas, whereas we observed no difference between the latencies recorded for white and grey matter stimulation. We can hypothesize that white matter stimulation enhances signal propagation in two different directions, resulting in an increase of observed connectivity probability. The locality of this effect suggests a dissipation of the signal propagating along antidromic pathways. This is an observation made at the cortex level that should be complemented by supplementary information about the connectivity at a more precise scale to be able to confirm this hypothesis.

5. Conclusion

We presented a new functional tractography atlas describing cortico-cortical connectivity of the human brain. Furthermore, we characterized dynamical properties of information flow between distant brain areas. Relevant functional complete maps for the scientific community are now available for download on f-tract. eu and will be regularly updated.

5.1. Consortium members

- Epilepsy Unit, Dept of Neurology, Pitié-Salpêtrière Hospital, APHP, Paris, France: Claude Adam, Vincent Navarro
- Neurology department, CHU, Rennes, France: Arnaud Biraben, Anca Nica, Dominique Menard
- Brno Epilepsy Center, Department of Neurology, St. Anne's University Hospital and Medical Faculty of Masaryk University, Brno, Czech Republic: Milan Brazdil, Robert Kuba, JitkaKočvarová, Martin Pail, Irena Doležalová
- Montreal Neurological Institute and Hospital, Montreal, Canada: François Dubeau, Jean Gotman
- Department of Functional Neurology and Epileptology, Hospices Civils de Lyon and University of Lyon, Lyon, France: Philippe Ryvlin, Jean Isnard, Hélène Catenoix, Alexandra Montavont, Sylvain Rheims
- Service de Neurophysiologie Clinique, APHM, Hôpitaux de la Timone, Marseille, France:Fabrice Bartolomei, Agnès Trébuchon, Aileen McGonigal
- Yuquan Hospital Epilepsy Center, Tsinghua University, Beijing, China: Wenjing Zhou, Haixiang Wang
- Canton Sanjiu Brain Hospital Epilepsy Center, Jinan University, Guangzhou, China: Sinclair Liu, Zhang Wei, Zhu Dan, GuoQiang, Hu Xiangshu, Li Hua, Hua Gang, Wang Wensheng, Mei Xi, Feng Yigang
- Department of Pediatric Neurosurgery, Hôpital Necker-Enfants Malades, Université Paris V Descartes, Sorbonne Paris Cité, Paris, France: Rima Nabbout, Marie Bourgeois, Anna Kaminska, Thomas Blauwblomme
- Multidisciplinary Epilepsy Unit, Hospital Universitario y Politécnico La Fe, Valencia, Spain: Vicente Villanueva Haba, Asier Gomez Ibanes, Antonio Gutierez Martin, Mercedes Garcés Sanchez

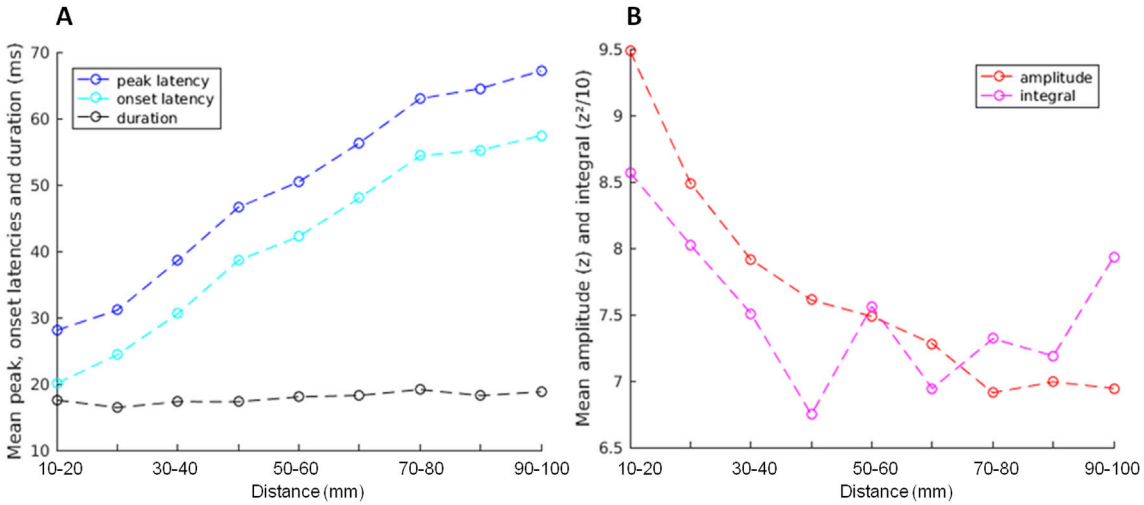

Fig. 10. Mean features values as a function of distance. (A) Dynamical features: onset and peak latencies, and duration. (B) Strength features: amplitude and integral.

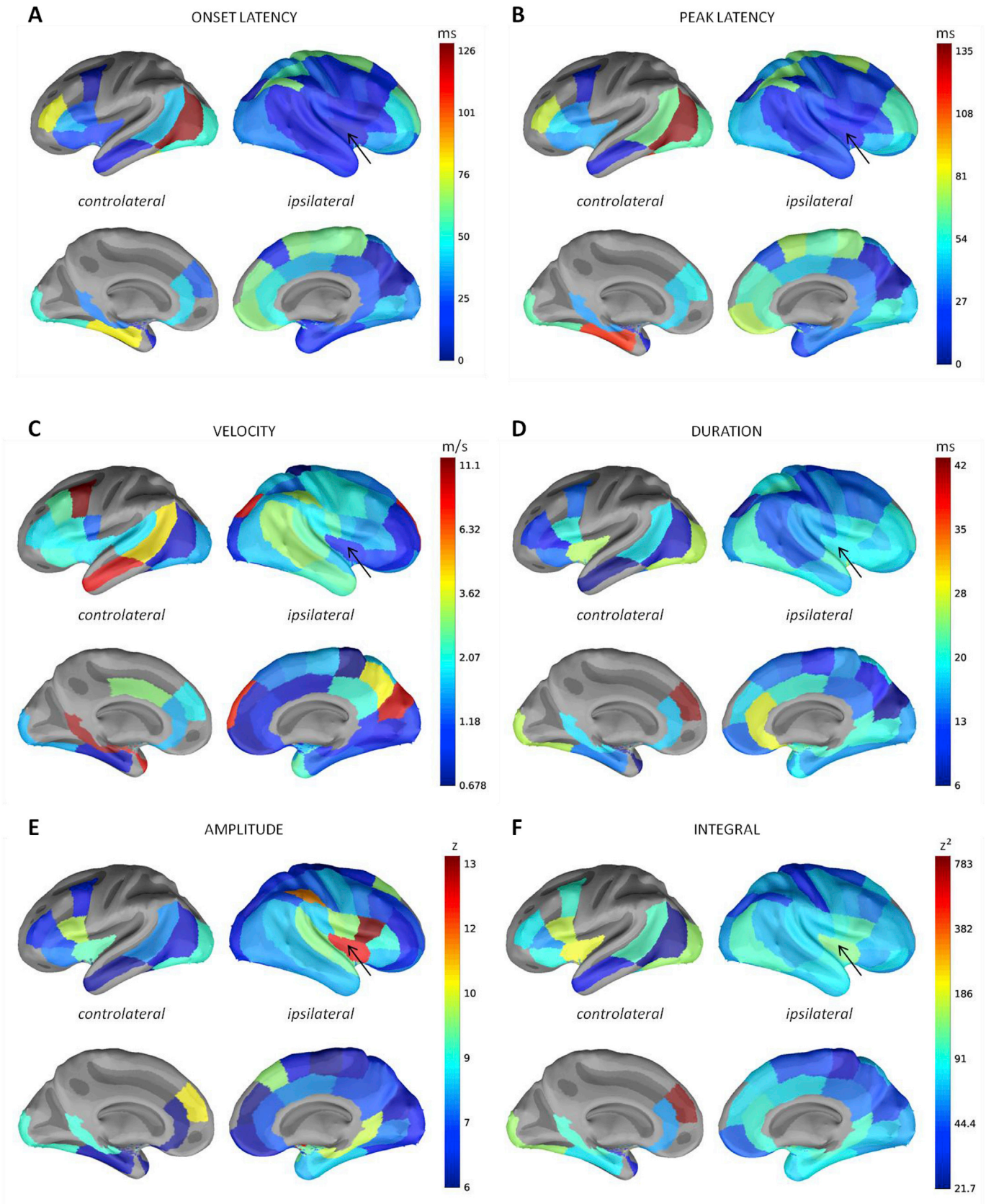

Fig. 11. Features computed for the stimulation of the insula (black arrow): the results were merged between the two hemispheres to represent ipsi- and controlateral connectivity. A log-scale was used to best display the values distribution of the velocity and the integral.

- Department of Neuroscience, Bambino Gesù Children's Hospital, IRRCS, Rome, Italy: Luca De Palma
- Department of Basic and Clinical Neuroscience, Institute of Psychiatry, Psychology & Neuroscience (IoPPN), London, UK: Antonio Valentin
- Epilepsy Unit, Hospital for Children and Adolescents, Helsinki, Finland: Liisa Metsähonkala, Eija Gaily, Leena Lauronen, Maria Peltola
- Department of Neurosurgery, Sainte-Anne Hospital, Paris, France: Francine Chassoux, Elizabeth Landré
- Epilepsy Unit, Department of Clinical Neurophysiology, Lille University Medical Center, Lille, France: Philippe Derambure, William Szurhaj, MaximeChochois
- University Hospital, Department of Neurology, Strasbourg, France: Edouard Hirsch, Maria Paola Valenti, Julia Scholly
- University Hospital, Department of Neurology, Toulouse, France: Luc Valton, Marie Denuelle, Jonathan Curot
- Epilepsy Monitoring Unit, Department of Neurology, Hospital del Mar-IMIM, Barcelona, Spain: Rodrigo Rocamora, Alessandro Principe, Miguel Ley
- Epilepsy Center, Medical Center – University of Freiburg, Faculty of Medicine, University of Freiburg, Germany: Andreas Schulze-Bonhage, Dirk-Matthias Altenmüller, Yulia Novitskaya
- Neurology Department, University Emergency Hospital, Bucharest, Romania: Ioana Mindruta, Andrei Barborica
- Epilepsy Surgery Center Niguarda Hospital, Milan, Italy: Stefano Francione, Roberto Mai, Lino Nobili, Ivana Sartori, Laura Tassi
- Centre Hospitalier Universitaire de Nancy, Nancy, France: Louis Maillard, Jean-Pierre Vignal, Jacques Jonas, Louise Tyvaert
- Service de neurochirurgie pédiatrique, Fondation Rothschild, Paris, France: Mathilde Chipaux, Delphine Taussig
- CHU Grenoble Alpes, Neurology Department, Grenoble, France: Philippe Kahane, LorellaMinotti, Anne-Sophie Job
- University Hospital, Department of Neurology, Bordeaux, France: Véronique Michel, Marie de Montaudoin, Jérôme Aupy
- CHU Bicêtre, Clinical Neurophysiology and Epileptology Unit, Kremlin-Bicêtre, France: Viviane Bouilleret, Ana Maria Petrescu, Pascal Masnou, Claire Dussaule, Marion Quirins

Acknowledgements

The research leading to these results has received funding from the European Research Council under the European Union's Seventh Framework Programme (FP/2007-2013) / ERC Grant Agreement n. 616268 “F-TRACT”. All the computations presented in this paper were performed using the CIMENT infrastructure (https://ciment.ujf-grenoble.fr), which is supported by the Rhône-Alpes region (GRANT CPER07_13 CIRA: http://www.ci-ra.org). We thank Bruno Bzenik and Romain Cavagna for their help on the CIMENT facility, and Jean-François Mangin and Cyril Poupon from Neurospin, CEA Saclay, for providing us with the ARCHI DTI database.

Appendix A. Supplementary data

Supplementary data related to this article can be found at https://doi.org/10.1016/j.neuroimage.2018.07.039.

References

Almashaikhi, T., Rheims, S., Ostrowsky-Coste, K., Montavont, A., Jung, J., De Bellescize, J., Arzimanoglou, A., Keo Kosal, P., Guénot, M., Bertrand, O., Ryvlin, P., 2014. Intrainsular functional connectivity in human. Hum. Brain Mapp. 35, 2779–2788. https://doi.org/10.1002/hbm.22366.

Ashburner, J., 2009. Computational anatomy with the SPM software. Magn. Reson. Imaging 27, 1163–1174. https://doi.org/10.1016/j.mri.2009.01.006.

Auzias, G., Coulon, O., Brovelli, A., 2016. MarsAtlas: a Cortical Parcellation Atlas for Functional Mapping, 37, pp. 1573–1592. https://doi.org/10.1002/hbm.23121.

Avants, B.B., Tustison, N.J., Wu, J., Cook, P.A., Gee, J.C., 2011. An open source multivariate framework for n-tissue segmentation with evaluation on public data. Neuroinformatics 9, 381–400. https://doi.org/10.1007/s12021-011-9109-y.

Besson, P., Bandt, S.K., Proix, T., Lagarde, S., Jirsa, V.K., Ranjeva, J.-P., Bartolomei, F., Guye, M., 2017. Anatomic consistencies across epilepsies: a stereotactic-EEG informed high-resolution structural connectivity study. Brain 1–14. https://doi.org/10.1093/brain/awx181.

Boido, D., Kapetis, D., Gnatkovsky, V., Pastori, C., Galbardi, B., Sartori, I., Tassi, L., Cardinale, F., Francione, S., de Curtis, M., 2014. Stimulus-evoked potentials contribute to map the epileptogenic zone during stereo-EEG presurgical monitoring. Hum. Brain Mapp. 35, 4267–4281. https://doi.org/10.1002/hbm.22516.

Brodmann, K., 1909. Vergleichende Lokalisationslehre der Grosshirnrinde. Johann Ambrosius Barth, Leipzig.

Catenoix, H., Magnin, M., Guénot, M., Isnard, J., Mauguière, F., Ryvlin, P., 2005. Hippocampal-orbitofrontal connectivity in human: an electrical stimulation study. Clin. Neurophysiol. 116, 1779–1784. https://doi.org/10.1016/j.clinph.2005.03.016.

Conner, C.R., Ellmore, T.M., DiSano, M.A., Pieters, T.A., Potter, A.W., Tandon, N., 2011. Anatomic and electro-physiologic connectivity of the language system: a combined DTI-CCEP study. Comput. Biol. Med. 41, 1100–1109. https://doi.org/10.1016/j.compbiomed.2011.07.008.

David, O., F-TRACT consortium, 2017. F-TRACT atlas. https://doi.org/10.18709/PERSCIDO.2017.10.DS166 version 1712. https://persyval-platform.univ-grenoble-alpes.fr/DS166/detaildataset.

David, O., Job, A.-S., De Palma, L., Hoffmann, D., Minotti, L., Kahane, P., 2013. Probabilistic functional tractography of the human cortex. Neuroimage 80, 307–317. https://doi.org/10.1016/j.neuroimage.2013.05.075.

Deco, G., Jirsa, V.K., McIntosh, A.R., 2013. Resting brains never rest: computational insights into potential cognitive architectures. Trends Neurosci. 36, 268–274. https://doi.org/10.1016/j.tins.2013.03.001.

Deman, P., Bhattacharjee, M., Rivière, D., Tadel, F., Cointepas, Y., David, O., 2018. IntrAnat Electrodes: a free database software to visualize intracranial electroencephalographic data in patient's referential and to initiate group studies. Front. Neuroinf. 12, 40. https://doi.org/10.3389/fninf.2018.00040.

Donos, C., Mălîia, M.D., Mîndruţă, I., Popa, I., Ene, M., Bălănescu, B., Ciurea, A., Barborica, A., 2016a. A connectomics approach combining structural and effective connectivity assessed by intracranial electrical stimulation. Neuroimage 132, 344–358. https://doi.org/10.1016/j.neuroimage.2016.02.054.

Donos, C., Mîndruţă, I., Ciurea, J., Mălîia, M.D., Barborica, A., 2016b. A comparative study of the effects of pulse parameters for intracranial direct electrical stimulation in epilepsy. Clin. Neurophysiol. 127, 91–101. https://doi.org/10.1016/j.clinph.2015.02.013.

Enatsu, R., Jin, K., Elwan, S., Kubota, Y., Piao, Z., O'Connor, T., Horning, K., Burgess, R.C., Bingaman, W., Nair, D.R., 2012a. Correlations between ictal propagation and response to electrical cortical stimulation: a cortico-cortical evoked potential study. Epilepsy Res. 101, 76–87. https://doi.org/10.1016/j.eplepsyres.2012.03.004.

Enatsu, R., Piao, Z., O'Connor, T., Horning, K., Mosher, J., Burgess, R., Bingaman, W., Nair, D., 2012b. Cortical excitability varies upon ictal onset patterns in neocortical epilepsy: a cortico-cortical evoked potential study. Clin. Neurophysiol. 123, 252–260. https://doi.org/10.1016/j.clinph.2011.06.030.

Enatsu, R., Kubota, Y., Kakisaka, Y., Bulacio, J., Piao, Z., O'Connor, T., Horning, K., Mosher, J., Burgess, R.C., Bingaman, W., Nair, D.R., 2013a. Reorganization of posterior language area in temporal lobe epilepsy: a cortico-cortical evoked potential study. Epilepsy Res. 103, 73–82. https://doi.org/10.1016/j.eplepsyres.2012.07.008.

Enatsu, R., Matsumoto, R., Piao, Z., O'Connor, T., Horning, K., Burgess, R.C., Bulacio, J., Bingaman, W., Nair, D.R., 2013b. Cortical negative motor network in comparison with sensorimotor network: a cortico-cortical evoked potential study. Cortex 49, 2080–2096. https://doi.org/10.1016/j.cortex.2012.08.026.

Enatsu, R., Gonzalez-Martinez, J., Bulacio, J., Kubota, Y., Mosher, J., Burgess, R.C., Najm, I., Nair, D.R., 2015. Connections of the limbic network: a corticocortical evoked potentials study. Cortex; a journal devoted to the study of the nervous system and behavior 62, 20–33. https://doi.org/10.1016/j.cortex.2014.06.018.

Entz, L., Tóth, E., Keller, C.J., Bickel, S., Groppe, D.M., Fabó, D., Kozák, L.R., Erőss, L., Ulbert, I., Mehta, A.D., 2014. Evoked effective connectivity of the human neocortex. Hum. Brain Mapp. 35, 5736–5753. https://doi.org/10.1002/hbm.22581.

Ercsey-Ravasz, M., Markov, N.T., Lamy, C., Van Essen, D.C., Knoblauch, K., Toroczkai, Z., Kennedy, H., 2013. A predictive network model of cerebral cortical connectivity based on a distance rule. Neuron 80, 184–197. https://doi.org/10.1016/j.neuron.2013.07.036.

Guevara, P., Duclap, D., Poupon, C., Marrakchi-Kacem, L., Fillard, P., Le Bihan, D., Leboyer, M., Houenou, J., Mangin, J.F., 2012. Automatic fiber bundle segmentation in massive tractography datasets using a multi-subject bundle atlas. Neuroimage 61, 1083–1099. https://doi.org/10.1016/j.neuroimage.2012.02.071.

Hagmann, P., Kurant, M., Gigandet, X., Thiran, P., Wedeen, V.J., Meuli, R., Thiran, J.-P., 2007. Mapping human whole-brain structural networks with diffusion MRI. PLoS One 2, e597. https://doi.org/10.1371/journal.pone.0000597.

Hagmann, P., Cammoun, L., Gigandet, X., Meuli, R., Honey, C.J., Wedeen, V.J., Sporns, O., 2008. Mapping the structural core of human cerebral cortex. PLoS Biol. 6, e159. https://doi.org/10.1371/journal.pbio.0060159.

Hammers, A., Allom, R., Koepp, M.J., Free, S.L., Myers, R., Lemieux, L., Mitchell, T.N., Brooks, D.J., Duncan, J.S., 2003. Three-dimensional Maximum Probability Atlas of the Human Brain, with Particular Reference to the Temporal Lobe, 19, pp. 224–247. https://doi.org/10.1002/hbm.10123.

Iwasaki, M., Enatsu, R., Matsumoto, R., Novak, E., Thankappen, B., Piao, Z., O'Connor, T., Horning, K., Bingaman, W., Nair, D., 2010. Accentuated cortico-cortical evoked potentials in neocortical epilepsy in areas of ictal onset. Epileptic Disord. 12, 292–302. https://doi.org/10.1684/epd.2010.0334.

Kahane, P., Tassi, L., Francione, S., Hoffmann, D., Russo Lo, G., Munari, C., 1993. [Electroclinical manifestations elicited by intracerebral electric stimulation "shocks" in temporal lobe epilepsy]. Neurophysiol. Clin. 23, 305–326.

Keller, C.J., Bickel, S., Entz, L., Ulbert, I., Milham, M.P., Kelly, C., Mehta, A.D., 2011. Intrinsic functional architecture predicts electrically evoked responses in the human brain. Proc. Natl. Acad. Sci. U.S.A. 108, 10308–10313. https://doi.org/10.1073/pnas.1019750108.

Keller, C.J., Honey, C.J., Entz, L., Bickel, S., Groppe, D.M., Tóth, E., Ulbert, I., Lado, F.A., Mehta, A.D., 2014a. Corticocortical evoked potentials reveal projectors and integrators in human brain networks. J. Neurosci. 34, 9152–9163. https://doi.org/10.1523/JNEUROSCI.4289-13.2014.

Keller, C.J., Honey, C.J., Mégevand, P., Entz, L., Ulbert, I., Mehta, A.D., 2014b. Mapping human brain networks with cortico-cortical evoked potentials. Philos. Trans. R. Soc. Lond. B Biol. Sci. 369 https://doi.org/10.1098/rstb.2013.0528, 20130528–20130528.

Kikuchi, T., Matsumoto, R., Mikuni, N., Yokoyama, Y., Matsumoto, A., Ikeda, A., Fukuyama, H., Miyamoto, S., Hashimoto, N., 2012. Asymmetric bilateral effect of the supplementary motor area proper in the human motor system. Clin. Neurophysiol. 123, 324–334. https://doi.org/10.1016/j.clinph.2011.06.011.

Koubeissi, M.Z., Lesser, R.P., Sinai, A., Gaillard, W.D., Franaszczuk, P.J., Crone, N.E., 2012. Connectivity between perisylvian and bilateral basal temporal cortices. Cerebr. Cortex 22, 918–925. https://doi.org/10.1093/cercor/bhr163.

Krieg, J., Koessler, L., Jonas, J., Colnat-Coulbois, S., Vignal, J.-P., Bénar, C.-G., Maillard, L.G., 2017. Discrimination of a medial functional module within the temporal lobe using an effective connectivity model: a CCEP study. Neuroimage 161, 219–231. https://doi.org/10.1016/j.neuroimage.2017.07.061.

Kubota, Y., Enatsu, R., Gonzalez-Martinez, J., Bulacio, J., Mosher, J., Burgess, R.C., Nair, D.R., 2013. In vivo human hippocampal cingulate connectivity: a corticocortical evoked potentials (CCEPs) study. Clin. Neurophysiol. 124, 1547–1556. https://doi.org/10.1016/j.clinph.2013.01.024.

Lacruz, M.E., Seoane, J.J.G., Valentin, A., Selway, R., Alarcón, G., 2007. Frontal and temporal functional connections of the living human brain. Eur. J. Neurosci. 26, 1357–1370. https://doi.org/10.1111/j.1460-9568.2007.05730.x.

Lacuey, N., Zonjy, B., Kahriman, E.S., Kaffashi, F., Miller, J., Lüders, H.O., 2015. Functional connectivity between right and left mesial temporal structures. Brain Struct. Funct. 220, 2617–2623. https://doi.org/10.1007/s00429-014-0810-0.

Mandonnet, E., Dadoun, Y., Poisson, I., Madadaki, C., Froelich, S., Lozeron, P., 2016. Axono-cortical evoked potentials: a proof-of-concept study. Neurochirurgie 62, 67–71. https://doi.org/10.1016/j.neuchi.2015.09.003.

Markov, N.T., Ercsey-Ravasz, M., Van Essen, D.C., Knoblauch, K., Toroczkai, Z., Kennedy, H., 2013. Cortical high-density counterstream architectures. Science 342. https://doi.org/10.1126/science.1238406, 1238406–1238406.

Matsumoto, R., Nair, D.R., LaPresto, E., Najm, I., Bingaman, W., Shibasaki, H., Lüders, H.O., 2004. Functional connectivity in the human language system: a cortico-cortical evoked potential study. Brain 127, 2316–2330. https://doi.org/10.1093/brain/awh246.

Matsumoto, R., Nair, D.R., LaPresto, E., Bingaman, W., Shibasaki, H., Lüders, H.O., 2007. Functional connectivity in human cortical motor system: a cortico-cortical evoked potential study. Brain 130, 181–197. https://doi.org/10.1093/brain/awl257.

Petkoski, S., Spiegler, A., Proix, T., Aram, P., Temprado, J.-J., Jirsa, V.K., 2016. Heterogeneity of time delays determines synchronization of coupled oscillators. Phys. Rev. E 94, 012209. https://doi.org/10.1103/PhysRevE.94.012209.

Ranck, J.B., 1975. Which elements are excited in electrical stimulation of mammalian central nervous system: a review. Brain Res. 98, 417–440.

Rivière, D., Geffroy, D., Denghien, I., Souedet, N., Cointepas, Y., 2009. BrainVISA: an extensible software environment for sharing multimodal neuroimaging data and processing tools. Neuroimage 47, S163. https://doi.org/10.1016/S1053-8119(09)71720-3.

Rosenberg, D.S., Mauguiere, F., Catenoix, H., Faillenot, I., Magnin, M., 2009. Reciprocal thalamocortical connectivity of the medial pulvinar: a depth stimulation and evoked potential study in human brain. Cerebr. Cortex 19, 1462–1473. https://doi.org/10.1093/cercor/bhn185.

Sporns, O., Tononi, G., Kötter, R., 2005. The human connectome: a structural description of the human brain. PLoS Comput. Biol. 1, e42. https://doi.org/10.1371/journal.pcbi.0010042.

Swadlow, H.A., 1989. Efferent neurons and suspected interneurons in S-1 vibrissa cortex of the awake rabbit: receptive fields and axonal properties. J. Neurophysiol. 62, 288–308.

Trebaul, L., Rudrauf, D., Job, A.-S., Mălîia, M.D., Popa, I., Barborica, A., Minotti, L., Mîndruţă, I., Kahane, P., David, O., 2016. Journal of neuroscience methods. J. Neurosci. Meth. 264, 94–102. https://doi.org/10.1016/j.jneumeth.2016.03.002.

Tuyisenge, V., Trebaul, L., Bhattacharjee, M., Chanteloup-Forêt, B., Saubat-Guigui, C., Mîndruţă, I., Rheims, S., Maillard, L., Kahane, P., Taussig, D., David, O., 2018. Automatic bad channel detection in intracranial electroencephalographic recordings using ensemble machine learning. Clin. Neurophysiol. 129, 548–554. https://doi.org/10.1016/j.clinph.2017.12.013.

Tzourio-Mazoyer, N., Landeau, B., Papathanassiou, D., Crivello, F., Etard, O., Delcroix, N., Mazoyer, B., Joliot, M., 2002. Automated anatomical labeling of activations in SPM using a macroscopic anatomical parcellation of the MNI MRI single-subject brain. Neuroimage 15, 273–289. https://doi.org/10.1006/nimg.2001.0978.

Umeoka, S., Terada, K., Baba, K., Usui, K., Matsuda, K., Tottori, T., Usui, N., Nakamura, F., Inoue, Y., Fujiwara, T., Mihara, T., 2009. Neural connection between bilateral basal temporal regions: cortico-cortical evoked potential analysis in patients with temporal lobe epilepsy. Neurosurgery 64, 847–855. https://doi.org/10.1227/01.NEU.0000344001.26669.92 discussion 855.

Valentín, A., Anderson, M., Alarcón, G., Seoane, J.J.G., Selway, R., Binnie, C.D., Polkey, C.E., 2002. Responses to single pulse electrical stimulation identify epileptogenesis in the human brain in vivo. Brain 125, 1709–1718.

Wilson, C.L., Isokawa, M., Babb, T.L., Crandall, P.H., 1990. Functional connections in the human temporal lobe. I. Analysis of limbic system pathways using neuronal responses evoked by electrical stimulation. Exp. Brain Res. 82, 279–292.

Yamao, Y., Matsumoto, R., Kunieda, T., Arakawa, Y., Kobayashi, K., Usami, K., Shibata, S., Kikuchi, T., Sawamoto, N., Mikuni, N., Ikeda, A., Fukuyama, H., Miyamoto, S., 2014. Intraoperative dorsal language network mapping by using single-pulse electrical stimulation. Hum. Brain Mapp. 35, 4345–4361. https://doi.org/10.1002/hbm.22479.